Check for updates

Chemical heterogeneity in interfacial layers of polymer nanocomposites†

Siyang Yang,[a] Siqi Liu, [ID][a] Suresh Narayanan, [ID][b] Chongfeng Zhang[a] and Pinar Akcora [ID] *[a]

It is well-known that particle–polymer interactions strongly control the adsorption and conformations of adsorbed chains. Interfacial layers around nanoparticles consisting of adsorbed and free matrix chains have been extensively studied to reveal their rheological contribution to the behavior of nanocomposites. This work focuses on how chemical heterogeneity of the interfacial layers around the particles governs the microscopic mechanical properties of polymer nanocomposites. Low glass-transition temperature composites consisting of poly(vinyl acetate) coated silica nanoparticles in poly(ethylene oxide) and poly(methyl acrylate) matrices, and of poly(methyl methacrylate) silica nanoparticles in a poly(methyl acrylate) matrix are examined using rheology and X-ray photon correlation spectroscopy. We demonstrate that miscibility between the adsorbed and matrix chains in the interfacial layers led to the observed unusual reinforcement. We suggest that packing of chains in the interfacial regions may also contribute to the reinforcement in the polymer nanocomposites. These features may be used in designing mechanically adaptive composites operating at varying temperature.

Introduction

Physically adsorbed chains on nanoparticles that form a strongly attractive interfacial layer exhibit different dynamics than that of bulk polymers. The strength of particle–polymer interactions change the conformations of the adsorbed chains and retard their mobility.[1–6] Chemical structure, molecular weight and rigidity of adsorbed polymers are important factors controlling the dynamic properties of interfacial layers.[7–10] The structural and dynamic properties of the interfacial layers, the trapped entanglements of free chains and the bridging between particles control the mechanical properties and reinforcement in polymer nanocomposites.[11–18] Most of these studies unravel the effect of an interfacial layer between the homopolymers and particles. In this study, dynamic heterogeneity of miscible blends with asymmetric composition in the presence of particles is examined through rheology and X-ray photon correlation spectroscopy.

Dynamic asymmetry in blends enriches the dynamic heterogeneities of interfacial polymers. We have recently shown that poly(methyl methacrylate), PMMA, adsorbed SiO_2 nanoparticles dispersed in poly(ethylene oxide), PEO, exhibited stiffening behavior as the temperature was swept around the glass-transition temperature (T_g) of PMMA.[17,19] The elastic hysteresis in the samples indicated that the adsorbed chains on the nanoparticles were stable after several heating–cooling steps.[17] These results revealed that the adsorbed chains did not exchange with the matrix chains during the temperature sweeps or long-time annealing.[4,14,17] A recent work also confirmed that the desorption of all adsorbed monomers from an attractive surface is energetically unfavorable.[20] In this work, we kept the adsorbed chains the same and changed the matrix polymer type to show that mixing of chemically different adsorbed and free chains with different T_g's influences the rheological behavior of nanocomposites. In particular, different lengths of poly(vinyl acetate), PVAc, chains adsorbed on particles in PEO and poly(methyl acrylate), PMA, matrices, are used to tune the dynamic properties. PVAc–PEO and PVAc–PMA are miscible polymers with binary interaction parameters of −0.011 and −0.3, respectively.[21–24] These attractive blends enable good mixing in the interface layers, which leads to good dispersion of the particles.

Our paper is structured as follows. First, the PVAc adsorbed chain length effects on the rheological properties of PEO composites T_g difference (ΔT_g) of 100 °C are presented and the unusual particle dynamics with the short adsorbed chains is discussed. Second, the system with a smaller ΔT_g (25 °C) between the same

[a] Department of Chemical Engineering & Materials Science, Stevens Institute of Technology, Hoboken, NJ 07030, USA. E-mail: pakcora@stevens.edu
[b] Advanced Photon Source, Argonne National Laboratory, Argonne, IL 60439, USA

† Electronic supplementary information (ESI) available: FTIR of PVAc adsorbed silica nanoparticles; DSC and XRD data of PVAc adsorbed in PEO matrices; loss tangent (tan δ) of 40 kDa PMA nanocomposites; SEM images of all 40 kDa PMA nanocomposites; time-temperature superposition of 40 kDa PMA nanocomposites with 50 kDa PVAc; temperature sweeps of 40 kDa and 140 kDa PMA composites; viscoelastic response of PMA homopolymers; viscoelastic data of 40 kDa PMA composites with varying adsorbed molecular weight; scattering model equations. See DOI: 10.1039/c8sm00663f

adsorbed chains in PMA matrix is presented with its rheology and XPCS results. Third, we showed in another amorphous composite system (PMMA adsorbed particles in the PMA matrix, ΔT_g: 98 °C) that the interfacial layer controlled reinforcement, observed in the PMA composite, is valid. The systematic study on changing the adsorbed and matrix molecular weights indicates that chemically heterogeneous systems have eminent potential to design thermally stiffening and mechanically adaptive composites. Large ΔT_g signifies the extent of dynamic heterogeneity between the adsorbed and matrix polymers and is here used to tune the mechanical properties of low-T_g polymer nanocomposites for applications such as high temperature resistant coatings.

Experimental section

Materials

PVAc of molecular weights 15 kDa (PDI: 2.6) and 50 kDa (PDI: 3.1) was purchased from Wacker Chemie AG, Germany. 100 kDa PVAc (PDI: 2.1) was purchased from Sigma-Aldrich. Colloidal SiO$_2$ nanoparticles in methylethylketone (50 ± 14 nm in diameter) were donated by Nissan Chemical America Corporation. –OH terminated 100 kDa PEO (PDI: 1.2) and 40 kDa PMA were purchased from Sigma-Aldrich. 140 kDa PMA and 118 kDa PMMA were synthesized by reversible addition–fragmentation chain-transfer polymerization (RAFT) using 2-[(dodecylsulfanyl)-carbonothioyl]sulfanyl propanoic acid (DCSPA) as a RAFT agent, and 2,2′-azobis(isobutyronitrile) (AIBN) as an initiator. The entanglement molecular weights of our polymers are lower than the molecular weights used. ($M_{e,PVAc}$: 10 kDa; $M_{e,PMMA}$: 10 kDa; $M_{e,PEO}$: 2 kDa; $M_{e,PMA}$: 8 kDa).

Determining the molecular weights of PMA

The hydrodynamic radius (R_h) of PMA in chloroform was obtained using a Zetasizer NanoS (Malvern Instruments) dynamic light scattering (DLS) instrument. The measurement duration was 13 s and the data were averaged over 11 runs. The R_g of a spherical particle was calculated from the measured R_h. It is known that $R_g/R_h \sim 1.2$ in a Θ-solvent and even greater in a good solvent.[25] Using $R_g \sim M^{0.6}$ of the polymer in good solvent and setting up the equations with respect to a known molecular weight of PMA at 40 kDa, $\langle R_{g,40}{}^2 \rangle / \langle R_g{}^2 \rangle = M_{40}{}^{1.2}/M^{1.2}$; $M = (R_{h,40}/R_h)^{5/3} (40\,000)$, we roughly estimated the molecular mass of the synthesized PMA as 140 kDa. $R_{g,40}$ is the radius of gyration and $R_{h,40}$ is the hydrodynamic radius of PMA at 40 kDa molecular weight.

The molecular weight of PMMA was measured in a gel permeation chromatography-light scattering (GPC/LS) instrument, equipped with a VARIAN PLgel 5.0 μm Mixed-C gel column (7.5 mm ID), a light detector (miniDawn, Wyatt Technology) and a refractive index detector (Optilab rEX, Wyatt).

Adsorbing polymers on the nanoparticles

Particles added to PVAc or PMMA solutions were mixed in a bath sonicator for 30 min and then stirred vigorously for 2 h. The particles were then collected by centrifuging at 8000 rpm for 5 min. The collected particles were washed 3 times in chlorobenzene and centrifuged to remove all free chains. The mass of

the adsorbed layers was determined using a thermal gravimetric analyzer (TA Instruments Q50). Measurements were carried out under 20 ml min^{-1} nitrogen flow at a heating rate of 20 °C min^{-1} between 30 and 550 °C. The samples were held at 150 °C for 20 min to remove residual solvent and heated up to 500 °C. The samples were run in a Bruker Tensor 27 Fourier transform infrared (FTIR) spectrometer to confirm the adsorbed chains on the particles. All spectra were collected in transmittance mode with a resolution of 4 cm^{-1}.

Nanocomposite preparation

PVAc- or PMMA-adsorbed nanoparticles in acetonitrile at 64 mg ml^{-1} were added to PEO or PMA matrix solution (25 mg ml^{-1} in acetonitrile) at specified particle loadings (10 and 30 wt%). The solutions were vigorously stirred for 40 min and cast in Teflon dishes in a fume hood for 12 h. The composite bulk films were annealed in a vacuum oven at 90 °C for 2 d.

Structural characterization

Scanning electron microscope (SEM) images were obtained using a Zeiss Auriga Dual-Beam FIB-SEM. The samples were frozen in liquid nitrogen for 15 min and fractured. Images were captured at different locations on the fracture surfaces at 1 kV beam and ∼5 mm working distance.

Thermal characterization

The crystallization temperature of PEO and the glass-transition temperatures of PVAc, PMA, PMMA and PEO homopolymers were measured in a Q100 DSC (TA Instruments). For PEO, the melting peak in the second heating cycle was integrated to obtain the heat of melting. The degree of crystallinity, X_c, was calculated using $X_c = \Delta H_m/\Phi \Delta H_m^0$, where ΔH_m^0 is the heat of melting of 100% crystalline PEO (196.8 J g^{-1}),[26] ΔH_m is the heat of melting and Φ is the volume fraction of PEO in the nanocomposites.

Rheological characterization

The viscoelastic properties of the nanocomposites were measured using a strain-controlled ARES-G2 rheometer (TA Instruments) equipped with 8 mm diameter stainless steel parallel plates. The nanocomposites were molded into 1 mm thick discs using our house-made compression molder at 80 °C under vacuum. In the temperature sweep experiments, the PEO composites were first heated to 80 °C and isothermally held for 10 min for complete melting, quenched to 30 °C at 15 °C min^{-1} cooling rate and equilibrated at 30 °C for 10 min to obtain good sample attachment to the rheometer fixtures. Temperature sweeps were performed in the linear regime for the whole temperature range at a frequency of 5 rad s^{-1} with 5 °C min^{-1} heating. The PMA composites were held at 30 °C for 10 min, and heated to 180 °C at 5 °C min^{-1}.

Modulus data were collected at a 0.2 Hz sampling rate. Frequency sweep tests were conducted at 85 °C and 1% strain amplitude in the linear regime. Time-temperature superposition (TTS) master curves of the PMA composites were obtained by shifting the 30 °C and 80 °C data with respect to the 55 °C reference temperature. The William–Landel–Ferry (WLF) equation was used for the TTS master

curves, $\log(\eta_T/\eta_{Tr}) = -C_1(T - T_r)/[C_2 + (T - T_r)]$. C_1 and C_2 are constants determined from the rheological shift factors, T_r is the reference temperature (55 °C) and η is the viscosity.

X-ray photon correlation spectroscopy (XPCS)

XPCS measurements were performed at the 8-ID-I beamline at the Advanced Photon Source, Argonne National Laboratory using 11 keV photon energy coherent X-rays. The normalized intensity auto-correlations were obtained over the wave vector range of 0.026–0.2 nm^{-1} at 36 discrete wave vector q values. The samples were held isothermally at the desired temperature for 30 min prior to the measurements, and then data were collected at five different locations, each 40 μm apart (beam area was 20 μm × 20 μm), to ensure that the data correlations represent dynamics of particles with uniform and stable dispersion. The PEO composites (10 and 30 wt%) were measured above their melting point at 80 °C. 30 wt% PVAc-adsorbed SiO$_2$ nanoparticles in the PMA composites were characterized at 160 °C. 15 kDa PVAc in 140 kDa PMA nanocomposites was characterized at 160 °C for about 4 h to confirm that the samples did not age over time. The measured intensity autocorrelation functions were fit to a stretched/compressed exponential model $f(q,t) = \exp[-(t/\tau)^\beta]$. PMMA adsorbed particles in PMA were run only in a rheometer.

Results and discussion

It is known that long chains strongly adsorbed on surfaces have a high fraction of segments in loops and tails.[27,28] The adsorbed polymer and matrix molecular weights of the prepared nanocomposites are given in Table 1. Colloidal SiO$_2$ nanoparticles (50 ± 14 nm) were physically adsorbed with PVAc (or PMMA) in chlorobenzene solution (30 mg PVAc/ml chlorobenzene). The adsorbed amounts of 15 kDa, 50 kDa and 100 kDa PVac chain lengths were measured to be 2.6, 2.8 and 3.2 wt%, respectively, in the thermal gravimetric analyzer (TGA). The number of chains (n) per particle is calculated as 166 for 15 kDa, 55 for 50 kDa and 33 for 100 kDa PVac, as shown in Fig. 1A. n is calculated from

$$n = \left(\frac{m_{ad}}{M_{ad}} \times N_a\right) \bigg/ \left(\frac{m_p}{\rho_p V_{1p}}\right),$$ where m_{ad} is the total adsorbed polymer mass from TGA; M_{ad} is the molecular weight of the adsorbed polymer; N_a is Avogadro's number; m_p is the total particle mass from TGA; ρ_p is the density of particles; V_{1p} is the volume of a single particle. The presence of adsorbed chains after three washes was confirmed by the presence of the carbonyl peak of PVAc in the FTIR of the particles (Fig. S1a, ESI†). A decrease in the intensity of the carbonyl absorbance peak for the supernatant indicates that the chains were not desorbed

after several washes (Fig. S1b, ESI†). The amount of adsorbed 118 kDa PMMA is measured to be 4.76 wt%.

The number of loops and train configurations change with increasing molecular weight of the adsorbed chains. Subsequently, the entanglements and dynamics of the free chains with the loops are influenced. It was recently reported that the thickness of the interfacial layer decreases with increasing chain length.[28] This unexpected result was explained by the lower packing of adsorbed and free chains in the interfacial layer,[28] but their impact on mechanical properties remains unexplored. Here, we suggest that the miscibility in blends, and thus packing of chains in the interphases, is controlled by both the molecular weight and different chemistry of the chains. Consequently, the density of the interfacial layer with chemical heterogeneities is conjectured to increase with decreasing molecular weight of the matrix chains. In the next section, we will address this point for two composite systems (PEO and PMA nanocomposites with good particle dispersion in both). We will present the effect of interfacial layers on the rheological properties and then on the particle relaxations of each nanocomposite listed in Table 1.

PVAc adsorbed SiO$_2$ nanoparticles in PEO matrices

The dispersion and distribution of PVAc-adsorbed silica particles in PEO (100 kDa) for two particle loadings (10 and 30 wt%) within the bulk samples were examined by SAXS and SEM. The SAXS data were collected during XPCS experiments and were modeled using a structure factor for hard spheres[29,30] along with the unified sphere form factor.[31,32] The model equations are presented in the ESI.† The fittings were performed using Igor software, Irena package. One population fitting with a Gaussian distribution was employed using the Modeling II mode. All the parameters, such as mean size and standard deviation in Gaussian distribution and the volume fraction in structure factor were fit together without fixing any parameter.

Table 2 summarizes the mean particle size, interparticle distance and particle volume fractions obtained from the fittings. The variation in the measured core size radius is within the range of dispersity obtained from the TEM image. The lower q feature seen in Fig. 1B samples at 0.0055 Å^{-1} is indicative of interparticle distance giving rise to a structure contribution to the SAXS data. The interparticle distance is consistently larger (~46 nm) for the 10 wt% than 30 wt% samples. The volume fractions (Φ_{vol}: 0.17) obtained from hard sphere structure fit were found to be larger than the actual volume fraction of silica fillers (10 wt% loading corresponds to $\Phi_{vol} \approx 0.05$). The volume fractions (Φ_{vol}: 0.18) obtained from structure model analysis coincide well with the actual particle loadings for the 30 wt%, which were equivalent to Φ_{vol}: 0.17 of silica particles. The SAXS

Table 1 Molecular weights (M.W.) and glass-transition temperatures (T_g) of the polymers used in the nanocomposites

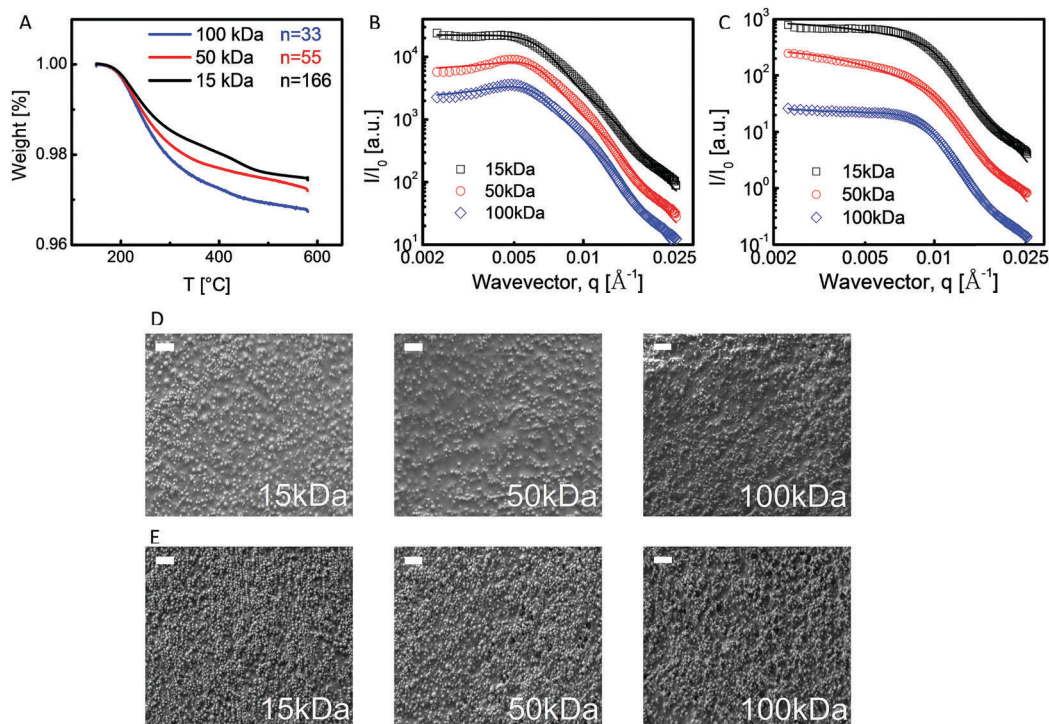| Matrix polymer	Adsorbed polymer	Composite, ΔT_g
PEO M.W.: 100 kDa, T_g: −65 °C	PVAc M.W.: 15, 50, 100 kDa T_g: 35 °C	100 °C
PMA M.W.: 40, 140 kDa, T_g: 10 °C		25 °C
PMA M.W.: 40, 110 kDa, T_g: 10 °C	PMMA M.W.: 118 kDa T_g: 108 °C	98 °C

Fig. 1 (A) TGA data of PVAc with varying molecular weights adsorbed on silica nanoparticles is used to determine the number of adsorbed chains on the particles (n). SAXS profiles of PEO nanocomposites with (B) 10 wt% and (C) 30 wt% silica nanoparticles adsorbed with PVAc of varying molecular weights: 15 kDa, 50 kDa and 100 kDa. Lines represent the model fits. SEMs of 15 kDa, 50 kDa and 100 kDa PVAc adsorbed particles in 100 kDa PEO matrices. Data are for composites with (D) 10 wt% and (E) 30 wt% particle loading. Scale bar is 500 nm.

Table 2 Primary particle size, inter-particle distance and volume fraction are obtained from the hard-sphere model along with unified sphere form factor fittings to the SAXS data of the PEO nanocomposites

Particle loading	Adsorbed chain M.W. (kDa)	Particle radius, r_s (nm)	Average inter-particle distance, r (nm)	Volume fraction, Φ_{vol}
10 wt%	15	31.9 ± 19.8	45.9	0.16
	50	34.7 ± 14.2	46.9	0.18
	100	33.8 ± 11.7	48.7	0.17
30 wt%	15	36.7 ± 12.6	29.6	0.20
	50	40.9 ± 15.6	28.6	0.18
	100	34.4 ± 6.8	29.5	0.17

data clearly show that particles were individually dispersed (Fig. 1B and C). At 30 wt% loading, the structure factor peaks at low q disappear, suggesting that the averaged interparticle spacings are not uniform as in 10 wt%, which may be the result of interparticle bridging. Fig. 1D and E present the SEMs of the samples characterized in SAXS.

We will discuss the rheology results of the 10 wt% samples first. The composite with the longer adsorbed chains (100 kDa PVAc in PEO) exhibited identical elastic modulus to the composite with bare particles (Fig. 2A). This result is indicative of the good miscibility between PEO and PVAc chains when they are at identical lengths. Interestingly, frequency sweeps show that the nanocomposite with the shortest adsorbed chain length (15 kDa PVAc) had a higher elastic modulus than the samples with the longer adsorbed chains at 85 °C (Fig. 2A). Mixing of short adsorbed and long free chains is energetically

more favorable, and thus the interphase is stronger as chain density and packing in the interphase region is conjectured to improve with the short chains, as also observed in a previous work where adsorbed and free chain chemistry is the same.[28] At 30 wt% particle loading, a similar trend was observed with the short adsorbed chains (Fig. 2B). The samples behaved solid-like ($G' > G''$) at this particle loading and 15 kDa and 50 kDa PVAc adsorbed nanocomposites had higher moduli in the glassy state. Slower softening behavior with temperature was consistent with the larger reinforcement obtained with the 15 kDa sample (Fig. 2C).

The effect of dynamic heterogeneities was more pronounced when the mobility of the adsorbed chains was modulated by the temperature. The temperature range in thermal sweeps was chosen between 30 and 55 °C, because we are interested in measuring how the composite behaves when adsorbed chains
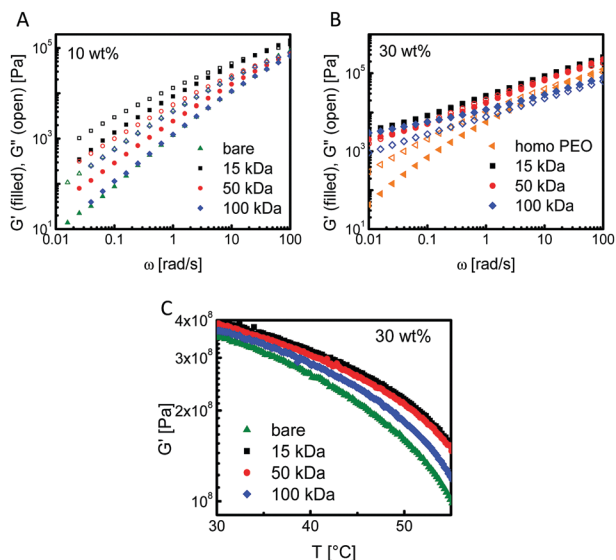
Fig. 2 Frequency sweeps of 100 kDa PEO homopolymer and its composites loaded with 15 kDa, 50 kDa, and 100 kDa PVAc-adsorbed and bare particles at 85 °C for (A) 10 wt% and (B) 30 wt% loadings. (C) Effect of adsorbed chain length on elastic modulus is observed in temperature sweeps at 1% strain and 5 rad s^{-1} frequency for 30 wt% loading.

become glassy and mobile by sweeping the temperature below and above the T_g of PVAc: 40 °C. The PEO matrix was semicrystalline during the measurements. The storage modulus of

PEO decreased only slightly with decreasing adsorbed chain length (Fig. 2C). Our bulk crystallinity data measured in DSC show that the adsorbed chain lengths did not influence the crystallinity of PEO (Fig. S2, ESI†) or the size of the PEO unit cell. XRD data analysis is shown in Fig. S3 (ESI†). Similar to the rheology protocol, the sample was heated and recrystallized and then reheated to measure the melting temperature in DSC. Since the degree of crystallization did not change with the adsorbed chain length, we propose that the rheological properties are solely governed by mixing of chains in interfacial layers within the amorphous regions of PEO.

In structured systems or composites with well-dispersed particles, XPCS measurements are used to explain the viscosity changes with nanoparticles or unusual reinforcement driven by interphases. In our recent XPCS study, we showed that the mobility of nanoparticles was controlled by the interfacial entanglements between grafted and matrix chains.[33] The XPCS results revealed that nanoparticles can feel the entanglements between grafted and free matrix chains, and hence particles at different dispersion states exhibited different dynamic modes.[33] Herein, particles adsorbed with PVAc of different chain lengths in PEO were run in XPCS to analyze the effect of interfacial layers on particle dynamics. Fig. 3A shows that the autocorrelation function of the composite with 15 kDa PVAc-adsorbed particles had a different relaxation mode than the other samples. The data were analyzed by fitting it to a double compressed exponential
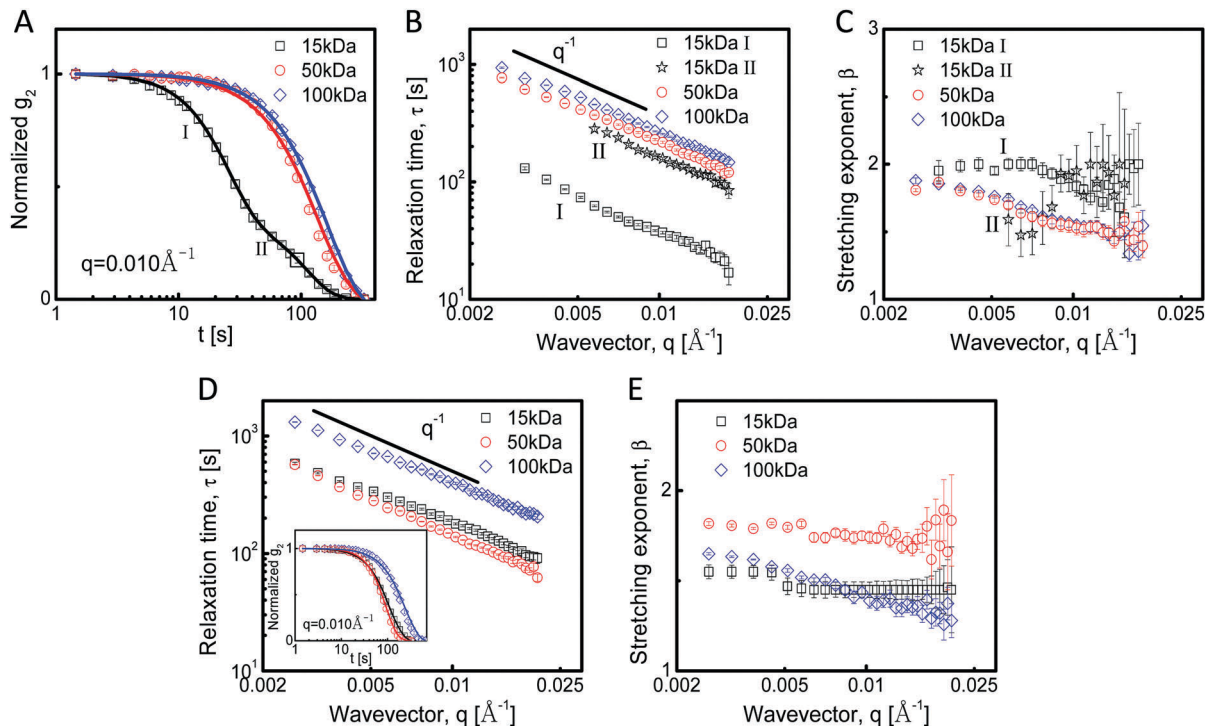

Fig. 3 Effect of adsorbed PVAc chain lengths (15 kDa, 50 kDa, 100 kDa) on nanoparticle dynamics: (A) autocorrelation function at q = 0.01 Å^{-1}, (B) relaxations times and (C) stretching exponent as a function of scattering vector, q. Samples are composites of 100 kDa PEO with 10 wt% loading. Data is collected at 80 °C. The 15 kDa sample has two different decay rates which are labeled as I and II in (A) and the relaxation times for the corresponding regions are shown in (B). (D and E) Relaxations and stretching exponent of particles adsorbed with PVAc of different chain lengths in 100 kDa PEO at 80 °C with 30 wt% loading. The inset in (D) shows the intensity autocorrelation function at q = 0.010 Å^{-1}.

model $g_2 = A + B_1 e^{-2\left(\frac{t}{\tau_1}\right)^{\beta_1}} + B_2 e^{-2\left(\frac{t}{\tau_2}\right)^{\beta_2}}$, where A is the baseline, B_1 and B_2 are the strengths of the two relaxations, τ is the relaxation time and β is the stretched/compressed exponent. The fast relaxation mode was attributed to the short chains dilating the highly dense (entangled) environment around the particle structures. Since we know that 15 kDa adsorbed chains reinforced the interphase layers, we propose that with the highly mobile short chains, the elastic modulus can be enhanced. This is consistent with what was concluded in our previous paper that the mobility of the adsorbed chains is essential for reinforcement.[17] The slow relaxation mode is attributed to the long PEO chains (100 kDa) in the heterogeneous interphase and is close to the relaxations of the 50 and 100 kDa samples (Fig. 3B). τ varies inversely with the wavevector q, $\tau \sim q^{-1}$, suggesting that particles move in hyper-diffusive mode in all three samples. The values of exponent β in Fig. 3C–E are indicative of hyper-diffusive dynamics. The nature of the hyper-diffusive dynamics still remains unclear, but previous studies have suggested that it can be caused by local heterogeneous stress relaxations.[34,35] At 30 wt% loading, the particles feel the network formed, and thus the dilation effect is not observed (Fig. 3D).

Recent calculations on the mobility of particles in entangled polymers suggest that local fluctuations of the entanglement meshes enable particles to hop between meshes.[36] It has been shown that the hopping of particles in high molecular weight polystyrene solutions was dictated by the sub-diffusive motion.[37] Diffusive motion of particles is suppressed when the particles are larger than the entanglement mesh size at times smaller than the entanglement time.[38] In our system, the particles are much larger than the matrix polymer mesh size and the mobility of the PVAc-adsorbed particles is measured to be hyper-diffusive in the molten state, which is seen in most of the jammed soft glassy systems and nanocomposites.[34,35,39] In summary, we demonstrate that mixing and entanglement between the two miscible polymers in the interphase layer is a factor governing the collective particle relaxations and the hyper-diffusive mode of adsorbed particles, which in turn contribute to the unusual reinforcement measured in the short adsorbed chains.

PVAc adsorbed SiO$_2$ nanoparticles in PMA matrices

PVAc–PMA is a miscible blend with strong polar interaction between the –O–CO– of PVAc and the –CO–O– of PMA.[24,40] The SAXS and SEM data showed that PVAc adsorbed SiO$_2$ nanoparticles were well dispersed in the 140 kDa PMA matrices (Fig. 4). The scattering model parameters are summarized in Table 3. The particle radius was found to be ~40 nm, which was independent of the adsorbed chain lengths. The model results reveal that particles were individually dispersed in all samples.

One way of tuning the compositional heterogeneity in the interphase layer is changing the matrix molecular weight. Linear rheology data of PVAc-adsorbed particles in 40 kDa and 140 kDa PMA show that the particles in the short matrix form a stronger elastic network (Fig. 5A) at long relaxation regimes. The reinforcement of this composite is attributed to the
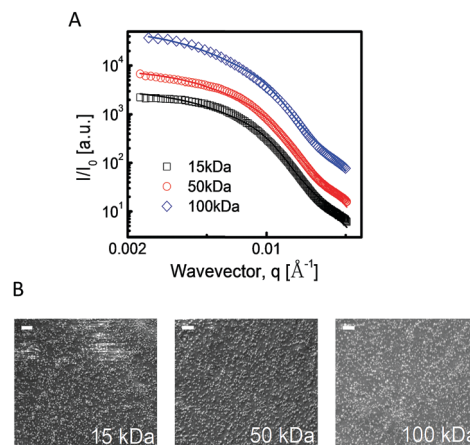

Fig. 4 (A) SAXS profiles of 140 kDa PMA nanocomposites with 30 wt% silica nanoparticles adsorbed with PVAc of varying chain lengths at 15 kDa, 50 kDa and 100 kDa. Lines are the model fits. (B) SEMs of 100 kDa PVAc-adsorbed particles in 140 kDa PMA matrices. Scale bar is 500 nm.

Table 3 Primary particle size; and structure factor parameters of average interparticle distance and volume fraction are obtained from hard-sphere model fittings to the SAXS data of PMA composites with 30 wt% loading

Adsorbed chain M.W. (kDa)	Particle radius, r_s (nm)	Average inter-particle distance, r (nm)	Volume fraction, Φ_{vol}
15	40.6 ± 16.1	28.4	0.15
50	40.1 ± 16.0	28.3	0.14
100	42.9 ± 18.3	27.8	0.15

good mixing and polar interactions between the short matrix and long adsorbed chains within the interphase volume. These factors can then enable effective bridging formed by the adsorbed chains. Temperature sweep experiments supported that composites with the short (40 kDa) PMA interestingly stiffen more than the long chains (140 kDa) (Fig. S4, ESI†). The interfacial mixing effect is evident when adsorbed particles are compared with the bare composite (Fig. 5A).
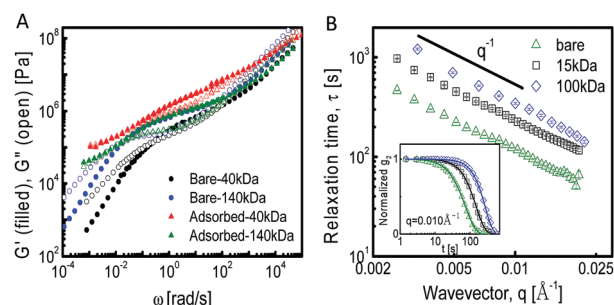

Fig. 5 (A) Effect of matrix molecular weight on the viscoelastic properties of PMA composites at a reference temperature of 55 °C. Molecular weights in the labels are for the matrix. The molecular weight of adsorbed PVAc is 50 kDa. (B) Relaxation times of 15 kDa and 100 kDa PVAc-adsorbed and bare nanoparticles in the 140 kDa PMA matrix. Data are collected at 160 °C. The inset shows the intensity autocorrelation function at $q = 0.010$ Å^{-1}. The particle loading is 30 wt% in all samples.
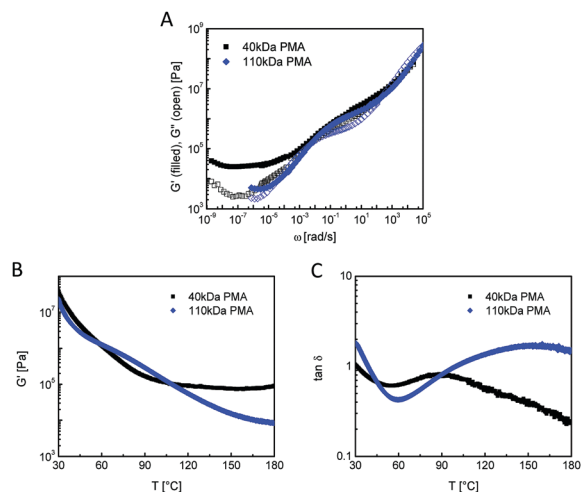
Fig. 6 Effect of matrix molecular weight on the viscoelastic properties of PMA composites. (A) TTS master curves of PMMA (118 kDa) adsorbed particles in 40 kDa and 110 kDa PMA at 30 wt% loading at a reference temperature of 55 °C. (B) Storage modulus and (C) tan δ in temperature sweeps of PMMA adsorbed nanoparticles in a 40 kDa and 110 kDa PMA matrix.

The reinforcement in the short matrix chains is better understood by comparing the linear viscoelastic responses of the PMA homopolymers. Obviously, larger moduli are obtained for the higher molecular weight of PMA at the same temperature or frequency (Fig. S5, ESI†). The opposite trend observed in the PMA composites with the PVAc adsorbed particles reveals the impact of chain packing within the interphases on the viscoelastic response, whereas the composites with bare particles present a similar trend to PMA homopolymers (Fig. 5A). Particles with long adsorbed PVAc chains can presumably feel the elastic environment of the interphase layer and particle relaxations are expected to become slower. The network forming effect of adsorbed particles is reflected in their slower particle relaxations (Fig. 5B), which is in-line with the relaxations of the PEO composites (Fig. 3B). The relaxation times of the particles increase with the adsorbed chain length.

We also looked into the adsorbed chain length effect in PMA (40 kDa) composites (Fig. S6 and S7, ESI†). The reinforcement effect and broadening of the rubbery plateau is clearly observed with the longer adsorbed chains. This reinforcement is attributed to the polar interactions between the two polymers. The subsequent dynamic coupling decreases the mobility of the matrix chains, and thereby enhances the mechanical properties of the nanocomposites. The plateau modulus at low frequency indicates network formation with the longer (100 kDa) adsorbed chains. The crossover of elastic and viscous moduli for the glass-rubber transition is at a lower frequency for the bare composites than for the PVAc-adsorbed composites and the rubber-liquid transition of the bare particles appears at a higher frequency (Fig. 5A). This indicates that some dynamic coupling between PVAc and PMA may be leading to faster glass-rubber relaxations.

PMMA adsorbed SiO₂ nanoparticles in PMA matrices

For better understanding of the PMA composite results, we changed the adsorbed polymer chemistry. Particles adsorbed

with PMMA (118 kDa) were dispersed in two different molecular weights of PMA matrix to prepare their composite with 30 wt% loading. The higher modulus value of the 40 kDa PMA composite at low frequencies indicates that the adsorbed particles in the short matrix formed a stronger elastic network (Fig. 6A). The stronger network is also seen in temperature sweeps (Fig. 6B), where the adsorbed particles were more reinforced particularly above the T_g of PMMA. The tan δ in Fig. 6C clearly shows that the 40 kDa PMA composite behaves more solid-like at high temperature and its tan δ decreases with increasing temperature. The elastic behavior at high temperature of this composite indicates that PMMA–PMA chains can dynamically couple as entanglements between adsorbed and matrix polymers yield a strong network formation.

Conclusions

We demonstrated that dynamic asymmetry and chemical heterogeneities in polymer blends control the mechanical properties of nanocomposites through the polymer–polymer interphases. A common finding from the three different systems is that good mixing of polymer blends resulted in reinforcement of the nanocomposites. In a semi-crystalline (PEO) matrix, the miscibility of short chains was more feasible with the amorphous chains and the highest reinforcement was obtained. The faster particle relaxations in the reinforced composite led us to conclude that adsorbed chain mobility is an important parameter in the reinforcement mechanism. In an amorphous (PMA) system, dynamic coupling, that was governed by entanglements and packing of chains in the interphase layer, was enhanced with the short matrix chains. Particle relaxations slowed down with the longer adsorbed chains, which in fact revealed the role of adsorbed chain length in the reinforcement mechanism. In summary, chemical heterogeneities at interphases control the reinforcement in the polymer composites. Our results underpin the polymer bridging effect through the interfacial layers which is shown to be more effective with the short matrix and long adsorbed chains. The demonstrated interfacially controlled reinforcement in low T_g polymer composites can be used to modulate mechanical properties at high temperature and shear.

Conflicts of interest

The authors declare no competing financial interest.

Acknowledgements

References

1 B. Metin and F. D. Blum, *J. Chem. Phys.*, 2006, **125**, 054707.

2 Y. Lin, L. Liu, G. Xu, D. Zhang, A. Guan and G. Wu, *J. Phys. Chem. C*, 2015, **119**, 12956–12966.

3 R. Bogoslovov, C. Roland, A. Ellis, A. Randall and C. Robertson, *Macromolecules*, 2008, **41**, 1289–1296.

4 E. Senses and P. Akcora, *Macromolecules*, 2013, **46**, 1868–1874.

5 C. C. Lin, S. Gam, J. S. Meth, N. Clarke, K. I. Winey and R. J. Composto, *Macromolecules*, 2013, **46**, 4502–4509.

6 S. Cheng, V. Bocharova, A. Belianinov, S. Xiong, A. Kisliuk, S. Somnath, A. P. Holt, O. S. Ovchinnikova, S. Jesse and H. Martin, *Nano Lett.*, 2016, **16**, 3630–3637.

7 B. Metin and F. D. Blum, *J. Chem. Phys.*, 2006, **124**, 054908.

8 D. N. Voylov, A. P. Holt, B. Doughty, V. Bocharova, H. M. Meyer III, S. Cheng, H. Martin, M. Dadmun, A. Kisliuk and A. P. Sokolov, *ACS Macro Lett.*, 2017, **6**, 68–72.

9 S. Cheng, B. Carroll, W. Lu, F. Fan, J.-M. Y. Carrillo, H. Martin, A. P. Holt, N.-G. Kang, V. Bocharova and J. W. Mays, *Macromolecules*, 2017, **50**, 2397–2406.

10 J. Moll and S. K. Kumar, *Macromolecules*, 2012, **45**, 1131–1135.

11 G. Heinrich, M. Klüppel and T. A. Vilgis, *Curr. Opin. Solid State Mater. Sci.*, 2002, **6**, 195–203.

12 S. Merabia, P. Sotta and D. R. Long, *Macromolecules*, 2008, **41**, 8252–8266.

13 A.-J. Zhu and S. Sternstein, *Compos. Sci. Technol.*, 2003, **63**, 1113–1126.

14 E. Senses and P. Akcora, *RSC Adv.*, 2014, **4**, 49628–49634.

15 A. Papon, H. Montes, F. Lequeux, J. Oberdisse, K. Saalwaechter and L. Guy, *Soft Matter*, 2012, **8**, 4090–4096.

16 S. Cheng, S. J. Xie, J. M. Y. Carrillo, B. Carroll, H. Martin, P. F. Cao, M. D. Dadmun, B. G. Sumpter, V. N. Novikov, K. S. Schweizer and A. P. Sokolov, *ACS Nano*, 2017, **11**, 752–759.

17 E. Senses, A. Isherwood and P. Akcora, *ACS Appl. Mater. Interfaces*, 2015, **7**, 14682–14689.

18 P. Akcora, S. K. Kumar, J. Moll, S. Lewis, L. S. Schadler, Y. Li, B. C. Benicewicz, A. Sandy, S. Narayanan, J. Ilavsky, P. Thiyagarajan, R. H. Colby and J. F. Douglas, *Macromolecules*, 2010, **43**, 1003–1010.

19 E. Senses, A. Faraone and P. Akcora, *Sci. Rep.*, 2016, **6**, 29326.

20 C. Yu and S. Granick, *Langmuir*, 2014, **30**, 14538–14544.

21 D. Fragiadakis and J. Runt, *Macromolecules*, 2009, **43**, 1028–1034.

22 A. N. Gaikwad, E. R. Wood, T. Ngai and T. P. Lodge, *Macromolecules*, 2008, **41**, 2502–2508.

23 J. Yin, G. Alfonso, A. Turturro and E. Pedemonte, *Polymer*, 1993, **34**, 1465–1470.

24 P. Casarino, A. Brunacci and E. Pedemonte, *Macromol. Chem. Phys.*, 1996, **197**, 3773–3782.

25 C. M. Kok and A. Rudin, *Macromol. Rapid Commun.*, 1981, **2**, 655–659.

26 H. Wang, J. K. Keum, A. Hiltner and E. Baer, *Macromolecules*, 2009, **42**, 7055–7066.

27 W.-Y. Lin and F. D. Blum, *Macromolecules*, 1998, **31**, 4135–4142.

28 S. Cheng, A. P. Holt, H. Wang, F. Fan, V. Bocharova, H. Martin, T. Etampawala, B. T. White, T. Saito, N.-G. Kang, M. D. Dadmun, J. W. Mays and A. P. Sokolov, *Phys. Rev. Lett.*, 2016, **116**, 038302.

29 S. R. Kline, *J. Appl. Crystallogr.*, 2006, **39**, 895–900.

30 J. K. Percus and G. J. Yevick, *Phys. Rev.*, 1958, **110**, 1.

31 A. Guinier, G. Fournet and C. Walker, *Small angle scattering of X-rays*, J. Wiley & Sons, New York, 1955.

32 G. Beaucage, *J. Appl. Crystallogr.*, 1995, **28**, 717–728.

33 S. Liu, E. Senses, Y. Jiao, S. Narayanan and P. Akcora, *ACS Macro Lett.*, 2016, **5**, 569–573.

34 S. Srivastava, P. Agarwal, R. Mangal, D. L. Koch, S. Narayanan and L. A. Archer, *ACS Macro Lett.*, 2015, **4**, 1149–1153.

35 H. Guo, G. Bourret, M. K. Corbierre, S. Rucareanu, R. B. Lennox, K. Laaziri, L. Piche, M. Sutton, J. L. Harden and R. L. Leheny, *Phys. Rev. Lett.*, 2009, **102**, 075702.

36 L. H. Cai, S. Panyukov and M. Rubinstein, *Macromolecules*, 2011, **44**, 7853–7863.

37 H. Guo, G. Bourret, R. B. Lennox, M. Sutton, J. L. Harden and R. L. Leheny, *Phys. Rev. Lett.*, 2012, **109**, 055901.

38 T. Ge, J. T. Kalathi, J. D. Halverson, G. S. Grest and M. Rubinstein, *Macromolecules*, 2017, **50**, 1749–1754.

39 J. P. Bouchaud and E. Pitard, *Eur. Phys. J. E: Soft Matter Biol. Phys.*, 2001, **6**, 231–236.

40 E. Princi, S. Vicini and E. Pedemonte, *Polym. Int.*, 2009, **58**, 656–664.